Tracking Charge Accumulation in a Functional Triazole-Linked Ruthenium-Rhenium Dyad Towards Photocatalytic Carbon Dioxide Reduction

Philipp Gotico, Thu-trang Tran, Aurelie Baron, Boris Vauzeilles, Christophe Lefumeux, Minh-huong Ha-thi, Thomas Pino, Zakaria Halime, Annamaria Quaranta, Winfried Leibl, et al.

Tracking Charge Accumulation in a Functional Triazole-Linked Ru-Re Dyad Towards Photocatalytic CO_2 Reduction

Philipp Gotico,[a] Thu-Trang Tran,[a] Aurelie Baron,[b] Boris Vauzeilles,[b] Christophe Lefumeux,[a] Minh-Huong Ha-Thi,[a] Thomas Pino,[a] Zakaria Halime,[c] Annamaria Quaranta,[b] Winfried Leibl,[b] Ally Aukauloo*[b][c]

[a] Dr. P. Gotico, Dr. T-T. Tran, C. Lefumeux, Dr. M-H. Ha-Thi, Dr. T. Pino
Université Paris Saclay, Institut des Sciences Moleculaire d'Orsay (ISMO)
91405 Orsay, France
[b] Dr. Z. Halime, Prof. A. Aukauloo
Université Paris Saclay, Institut de Chimie Moléculaire et des Matériaux d'Orsay (ICMMO)
91405 Orsay, France
[c] Dr. A. Baron, Dr. A. Quaranta, Dr. W. Leibl, Prof. A. Aukauloo
Université Paris Saclay, CEA, Institut de Biologie Intégrative de la Cellule (I2BC)
91191 Gif-sur-Yvette, France
Email: ally.aukauloo@universite-paris-saclay.fr

Supporting information for this article is given via a link at the end of the document.

Abstract: A novel triazole-linked ruthenium photosensitizer and rhenium catalyst dyad was synthesized and investigated for photo-induced charge accumulation using pump-pump-probe transient absorption spectroscopy. The triazole bridging ligand promoted weak electronic communication between the two units, resulting in an anodic shift of the reduction potentials of the Re moiety. Upon excitation, the first charge-separated state is formed at an apparent rate of 5.4×10^7 s^{-1}, however a second excitation resulted in an efficient intramolecular reverse electron transfer preventing the two-electron accumulation in the catalyst. Under continuous irradiation and use of sacrificial electron donors, photocatalytic CO_2 reduction activities show good turnover numbers boosted by the effect of the sacrificial electron donor.

Introduction

Reduction of carbon dioxide (CO_2) into energy-rich compounds using solar light as an energy source provides a sustainable approach in solving the problem of global warming. Natural photosynthesis provides us with the scheme of how to use the abundant resources of water, CO_2, and sunlight for the production of energy-rich carbohydrates. Mimicking this scheme usually involves synthesizing supramolecular assemblies that contain a photosensitizer (PS) able to harnesses solar energy, creating charge separated states, where the holes are used by oxidation catalysts to oxidize water to oxygen, and electrons are used by reduction catalysts to reduce CO_2 into gaseous or liquid fuels.

One of the well-studied systems for photocatalytic CO_2 reduction involves the rhenium carbonyl diimine complexes first reported by Lehn.[1,2] The great activity of the system stems from its robustness, efficiency, and the inherent selectivity of the doubly-reduced active form towards the CO_2 substrate even in the presence of excess protons in the solution, favoring the production of CO from CO_2 over the notoriously competing proton reduction to hydrogen gas.[3] This complex is also considered as a "photo"-catalyst but requires a high-energy excitation in the ultraviolet region. As such, improvements on such systems include modification of the diimine and peripheral ligands to enhance catalysis and to shift the absorption properties into the visible range.[4–10] Better performances were achieved by incorporating photosensitizers, with the archetypal ruthenium trisbipyridine (**Ru**), in supramolecular assemblies, to photo-activate the Re catalyst in the visible spectral window as shown in Scheme 1. In this strategy, the choice of the linker/bridging ligand (**L**) is important as it plays important roles in conveying efficiently the electrons in an unidirectional fashion from the photosensitizer to the catalyst, and helping to maintain a spatial and temporal charge accumulation in the latter for the eventual use in the multi-electronic catalytic CO_2 reduction.

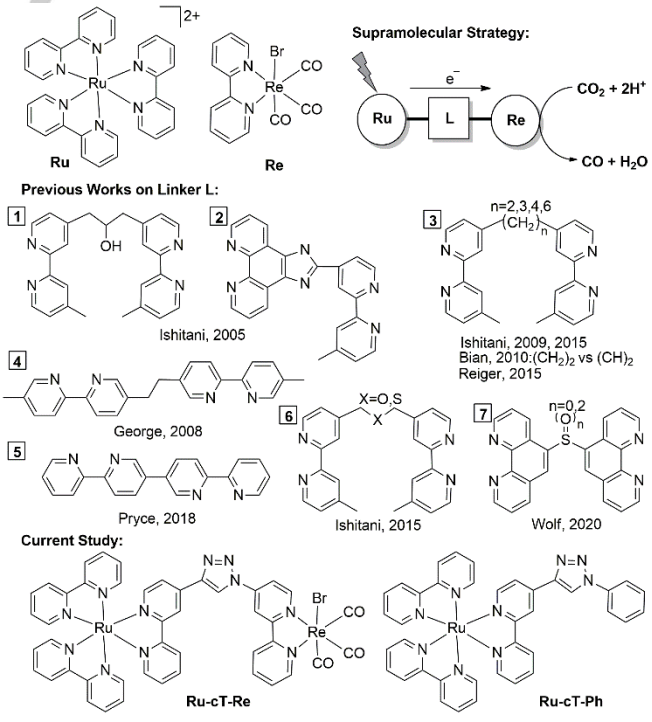

Scheme 1. Supramolecular strategy to link a Ruthenium photosensitizer and a Rhenium catalyst (top) using previously reported bridging ligand and the Ru-Re dyad system investigated in this study (bottom).

Supramolecular catalysts comprising such **Ru** photosensitizer and **Re** catalyst have been extensively studied by the group of Ishitani.[11,12] The highest photocatalytic turnover number (TON = 3000) was achieved for a dyad containing $[Ru(dmb)_3]^{2+}$ and $Re(dmb)(CO)_2(PPhF_3)_2$ (dmb = 4,4'-dimethyl-2,2'-bipyridine) linked through a saturated ethyl group (linker **3** with n = 2), in dimethylformamide using 1,3-dimethyl-2-phenyl-2,3-dihydro-1H- benzo[d]imidazole (BIH) as a sacrificial electron donor (SED).[13] It has been suggested by the group of Bian that the introduction of a conjugated linker between the diimine moieties, such as CH_2=CH_2 in ligand **3** decreases the photocatalytic activity because bond conjugation lowers the π*-orbital energy level of the Re catalyst unit which consequently decrease its reduction power.[14,15] Similar results were obtained with the conjugated linker **2** regardless of the positioning of the Ru and Re moieties in either the phenanthroline or bipyridine groups, showing much inferior activities than their bimolecular counterparts.[16] As such, weaker electronic communication, as observed in saturated alkyl chain bridges in **1** and **3**, even though displaying almost isoenergetic thermodynamic drive for the first electron transfer, were the mostly recommended and used bridge in designing supramolecular assemblies.[13,17–24] Ishitani and colleagues have investigated the intramolecular electron transfer in these systems, using time-resolved infrared absorption measurements in the presence of irreversible electron donors, and showed a very rapid electron transfer ($>2\times10^7$ s^{-1}), confirming that such saturated linkers adequately transfer photo-produced electrons to the catalyst unit.[25]

Elaborating further on bridging ligand design, it was found that increasing the alkyl chain length from two carbon atoms to four or six, lowered the photocatalytic activity.[20] On the other hand, positioning the linker in the meta positions of the bipyridine ring and removing the alkyl chain bridge as in linker **5** induces a weak electronic communication between the metal centers and showed lower photocatalytic activity than their bimolecular counterpart.[26] Decorating the alkyl linker with an electronegative oxygen atom as in **6** increased the thermodynamic drive for the first electron transfer from Ru to Re compared to its carbon analogue, and consequently gave better photocatalytic activities.[27] Replacing the oxygen with a sulfur atom in linker **6,** however, resulted to a less stable system as the dyad splits into its mononuclear forms during photo-irradiation. Recently, the group of Wolf reported an enhanced photocatalytic activity when using an oxidized sulfone group (SO_2) in linker **7** compared to its sulfide analogue and attributed enhancement to better electronic communication between the metal centers, resulting in positive shifts of the reduction potentials.[28] However, the system faced similar photo-degradation concerns indicating the vulnerability of the C-S bond.

From these investigations on different bridging ligands, there appears to be an unexpected contradiction to the rationale of a supramolecular design in creating an efficient flow of electron from the photosensitizer unit to the catalyst. On one hand, the use of linkers promoting strong electronic communication accelerates electron transfer from the photosensitizer to the catalyst but results in lowered photocatalytic activities, while on the other hand, saturated alkyl linkers provide better photocatalytic activities even with low thermodynamic drive for the first photo-induced electron transfer. This counter-intuitive results possibly suggests that the rate-limiting step in the photocatalytic CO_2 reduction in these systems is not the first electron transfer but the subsequent steps (catalyst-centered processes such as halide loss, two-electron accumulation forming the doubly-reduced active form, interaction of the active form with the substrate, and succeeding protonation and electron transfer steps).[29–31] As the previous systems mostly focused on the effect of the bridging ligand on the formation of the one-electron reduced species (OERS) of the Re catalyst, the thermodynamics and kinetics of the photo-induced formation of the catalytically active doubly-reduced form of the catalyst is seldom reported. To address this point, in this study we synthesized a new Ru–Re dyad linked by a triazole moiety (**Ru-cT-Re**) and investigated its photophysical and photocatalytic properties. The triazole linker is a common bridge for supramolecular systems readily prepared by "click" chemistry, a simple and efficient covalent ligation methodology.[32] Moreover, it has been reported to promote good electron transfer in supramolecular dyads and the rigidity of such bridge prevents any unwanted charge transfer.[33–35] We investigated the first photo-induced electron transfer from the Ru photosensitizer to the Re catalyst using nanosecond laser flash photolysis and for the first time attempted to track the photo-induced two-electron accumulation in the Re moiety. Together with photocatalytic optimizations, our results provide critical implications of supramolecular design, especially if such strategies will be employed in hybrid interfaces of photo-electrochemical cells.

Results and Discussion

Synthesis

The **Ru-cT-Re** dyad was synthesized using the copper-catalyzed azide–alkyne cycloaddition (popularly known as 'click' chemistry) starting from the versatile Ru-C≡CH synthon (compound **A**, Scheme 2)[35] and an azide-substituted bipyridine ligand used in the next step to introduce the Re triscarbonyl catalyst (Scheme 2). Similar strategy has been utilized for the facile incorporation of various catalytic and donor/acceptor units to a photosensitizer,[33,33–36] with the Ru-Ni cyclam dyad been the most relevant for photocatalytic CO_2 reduction.[37]

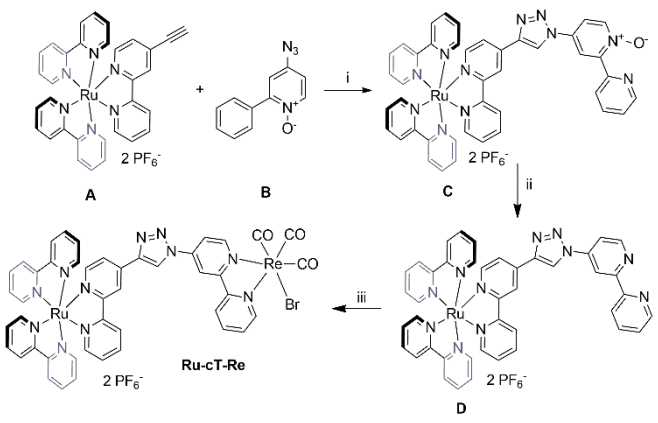

Scheme 2. Synthetic route for the preparation of the **Ru-cT-Re** dyad. Reagents and conditions: (i) $CuSO_4.5H_2O$, sodium ascorbate, CH_2Cl_2/H_2O (77%); (ii) PCl_3, CH_2Cl_2 (79%); (iii) $[Re(CO)_5Br]$, THF/CH_3CN (86%).

Absorption and Emission Properties

The absorption spectrum of the **Ru-cT-Re** dyad displays absorption features characteristic of both mononuclear complexes **Ru-cT-Ph** and **Re** (Figure 1a). The strong ^{1}MLCT absorptions between 400 and 500 nm (peak at 464 nm), characteristic of the Ru(II) unit, is clearly visible in the spectrum whereas the weaker higher energy ^{1}MLCT absorption characteristic of the Re(I) terminus is apparent as an increased absorbance in the 350 – 400 nm region. Compared to the **Re** catalyst alone, the extended absorption of the **Ru-cT-Re** dyad in the visible range is beneficial for photocatalytic applications as the strong absorption at 400 – 500 nm coincides with the intense irradiance from the solar spectrum. The triazole linker between the photosensitizer and the catalyst resulted in (i) a slight red-shift in the absorption spectra, and (ii) increased absorption in the dyad as compared to the spectral summation of the **Ru-cT-Ph** and **Re** reference complexes. These spectral changes are characteristic of a weak electronic communication between the two metals in the system.[14,16] The emission spectrum of the **Ru-cT-Re** shows an absorption maximum at 633 nm corresponding to the triplet metal-to-ligand charge transfer (^{3}MLCT) excited state of the Ru moiety exhibiting a long-lived lifetime of 1085 ns (Table 1). This **Ru-cT-Re** emission is 5 nm red-shifted compared to the **Ru-cT-Ph** reference but 20 nm red-shifted compared to the **Ru** reference. Both the triazole-linked **Ru-cT-Re** dyad and **Ru-cT-Ph** reference have longer-lived emission lifetimes and higher emission quantum yields compared to the **Ru** reference, and we have previously ascribed this to the partial delocalization of the LUMO on the triazole-linked bipyridine.[35] The similarity of the excited state lifetimes of **Ru-cT-Re** and **Ru-cT-Ph** indicates that no energy or electron transfer occurred from the excited state of Ru moiety to the Re moiety.

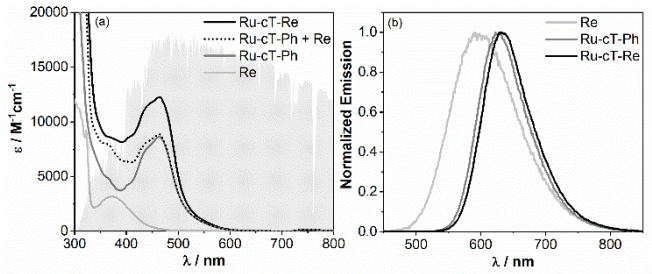

Figure 1. Absorption spectra of **Ru-cT-Re** in comparison with mononuclear references **Ru-cT-Ph** and **Re**. Dotted lines show spectral summation of the reference complexes. Shaded area represents solar irradiation spectrum. (b) Normalized emission spectra of the complexes in Ar-degassed ACN/H_2O.

Table 1. Emission data of the complexes studies in Ar-degassed ACN/H_2O.

Complex	λ_{abs} / nm	λ_{em} / nm	τ / ns	Φ_{em}
Ru-cT-Re	464	633	1085	0.113
Ru-cT-Ph	464	628	1081	0.097[35]
Ru	454	612	900	0.059[38]
Re	372	599	25	0.005[39]

Table 2. Redox potentials ($E_{1/2}$) of the complexes in Ar-saturated acetonitrile with 100 mM TBAP measured in V *vs* $Fc^{0/+}$.

Complex	$Re^{II/I}$	$Ru^{III/II}$	$ReL^{0/-}$	$Re^{I/0}L^{0/-}$	$RuL^{0/-}$	$RuL^{-/2-}$	$RuL^{2-/3-}$
Ru-cT-Re	1.01[a]	0.87	-1.56[a]	-1.98[b]	-1.76	-1.98[b]	-2.24
Ru-cT-Ph	-	0.84	-	-	-1.75	-1.96	-2.20
Ru	-	0.85	-	-	-1.77	-1.97	-2.20
Re	0.92[a]	-	-1.78	-2.10	-	-	-

[a] Peak potential of irreversible peak. [b] Two-electron peak

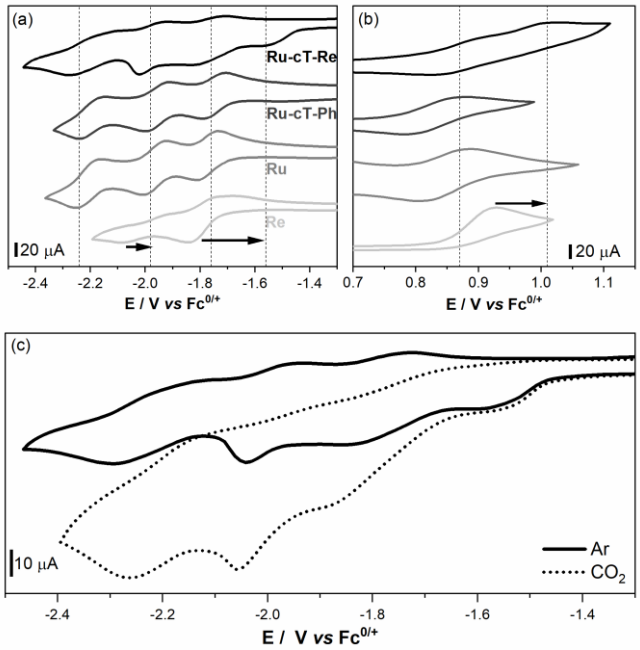

Figure 2. CVs showing (a) reduction and (b) oxidation potentials of **Ru-cT-Re** dyad (black) in comparison with **Ru-cT-Ph**, **Ru**, and **Re** in Ar and (c) in CO_2-saturated ACN solution containing 100 mM TBAP. Dashed lines in (a) and (b) correspond to potentials of **Ru-cT-Re** reported in Table 2. Arrows indicate the shift of the Re-related redox peaks in **Ru-cT-Re**.

Electrochemical Characterization

The cyclic voltammograms (CV) in Figure 2 show characteristic oxidation and reduction waves of the **Ru-cT-Re** dyad and of the mononuclear reference complexes **Ru-cT-Ph**, **Ru**, and **Re**. Two oxidation waves were observed for the heterometallic complex **Ru-cT-Re**: (i) a first reversible oxidation wave at 0.87 V attributed to $Ru^{III/II}$ and (ii) a second $Re^{II/I}$ irreversible peak at 1.01 V due to the rapid bromine loss (Figure 2b, Table 2). Both peaks were shifted anodically in the dyad compared to the

mononuclear complexes possibly due to the presence of another metal asserting an electron withdrawing effect. It is observed however, that the Ru moiety is not significantly shifted compared to the 90 mV shift displayed for the Re moiety.

The three reduction waves of the **Ru-cT-Ph** at -1.75 V, -1.96 V, and -2.20 V are attributed to the reduction of the three bipyridyl ligands, similar to the three reduction potentials of **Ru**, (Figure 2a, Table 2). The presence of the triazole linker in **Ru-cT-Ph** did not significantly shift the reduction potentials of **Ru**. Similarly, the reduction potentials at -1.76 V, -1.98 V, and -2.24 V of the **Ru-cT-Re** dyad complex are attributed to the bipyridyl reductions of the Ru moiety. The small shifts in the reduction potential of the Ru moiety are consistent with the shifts observed in oxidation. These results indicate that the triazole bridging with the Re catalyst did not significantly affect the redox properties of Ru photosensitizer.

The first reduction potential of **Ru-cT-Re** observed at -1.56 V is attributed to the reduction of the bipyridyl ligand of rhenium moiety. This is confirmed by the following comparisons: (i) the wave is irreversible possibly due to ligand loss (Br^-) in the rhenium which is similarly observed for the mononuclear **Re** complex, (ii) a catalytic wave is observed just after this wave when the solution is saturated with CO_2 (Figure 2c) indicating the electrocatalytic activity of the Re moiety towards CO_2 reduction, and (iii) the wave is observed neither for **Ru-cT-Ph** nor for **Ru** reference complexes and therefore can only come from the Re moiety. The large anodic shift (220 mV) of the reduction potential of the Re moiety in the **Ru-cT-Re** dyad complex is consistent with the observed anodic shift of the Re oxidation potential but the effect is stronger for the reduction potential because it is a bipyridyl-centered reduction. Since the first reduction potential of the Re moiety is less negative than that of the Ru moiety, intramolecular electron transfer from the reduced Ru moiety to the Re moiety in the ground state should proceed smoothly (ΔG = -220 meV). The second reduction of the Re moiety, reported to be a metal-centered reduction, is expected to occur at -1.98 V in the dyad due to the 2-electron nature of the reduction wave. As such, it can be expected that there will be an uphill thermodynamic drive (ΔG = +220 meV) for the second electron accumulation in the Re moiety from the reduced Ru.

Tracking the First Charge Separated State (1st CSS)

The activation of the **Re** catalyst by the **Ru** photosensitizer was previously investigated by our group in a bimolecular system with sodium ascorbate (**Asc**) as a reversible electron donor in Ar-saturated ACN/H_2O solution.[40] We have utilized nanosecond transient absorption spectroscopy and upon detailed spectroscopic and kinetic analyses, we were able to distinguish the bipyridyl-based reductions between **Ru** and **Re**. The one-electron reduced species (OER) of **Ru** has a characteristic transient absorption at 510 nm, and although the OER of **Re** has similar transient absorption in this same region, it also possesses an additional absorption at 450 nm where the OER of **Ru** would otherwise have a bleaching. Therefore, following the absorption changes at these wavelengths, we were able to estimate a diffusion-limited electron transfer rate of 4.8×10^9 $M^{-1}s^{-1}$ from the OER of **Ru** to **Re**, even though there is almost an isoenergetic thermodynamic drive for this process (ΔG ~ +10 meV).

The **Ru-cT-Re** dyad was similarly investigated here and the transient absorption spectra at various delay times are shown in Figure 3. At these short time scale (0 – 100 ns), the transient spectra are characterized by an initial depletion of the Ru ground-state MLCT band at 450 nm, followed by an intense absorption growth at 400 – 600 nm region. In comparison with the transient absorption spectra of **Ru-cT-Ph** (Figure S1), one distinct observation is the formation of positive absorption at 450 nm, which is consistent with the OER of Re, formed upon fast intramolecular electron transfer.

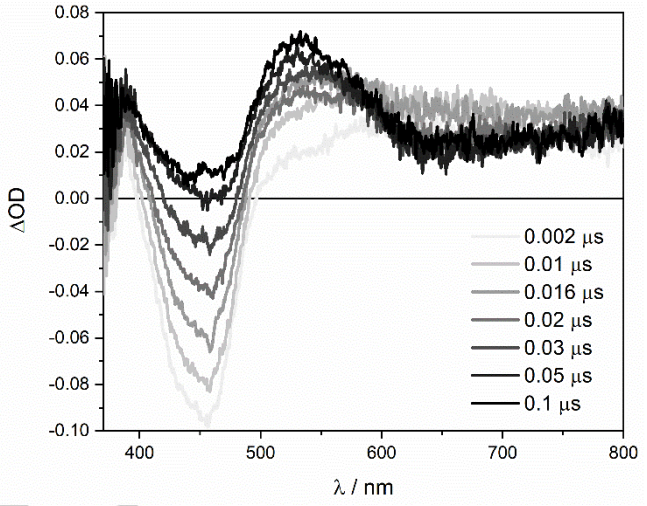

Figure 3. Transient absorption spectra of **Ru-cT-Re** (57 μM) and Asc (100 mM) in Ar-saturated ACN/H_2O in various delay times after single-pulse excitation at 460 nm (6.5 mJ per pulse).

Figure 4. Transient absorption decays at selected wavelengths of **Ru-cT-Re** (57 μM) and Asc (100 mM) in Ar-saturated ACN/H_2O after single-pulse excitation at 460 nm (6.5 mJ per pulse). Inset: decay-associated difference spectra: 19 ns attributed to decay of Ru^{II}*-cT-Re^{I} and *c* attributed to transient spectra of 1st CSS.

The kinetic traces at representative wavelengths are shown in Figure 4, and provide a clear picture of the mechanism of the first photo-induced charge-separation process. Upon laser excitation and formation of the excited state Ru^{II}*-cT-Re^{I} (bleaching at 450 nm), the species relaxes to concomitantly give oxidized $Asc^{\cdot+}$ at 390 nm and the OER of Re (formal Re^0 species) with characteristic absorption at 450 nm and 500 nm. This is indicative of a first electron transfer between Asc and Ru^{II}*-cT-Re^{I} to give $Asc^{\cdot+}$ and Ru^{I}-cT-Re^{I} (OER of Ru moiety). The latter then undergoes a very fast intramolecular electron transfer to form Ru^{II}-cT-Re^0. The kinetic traces are globally fitted

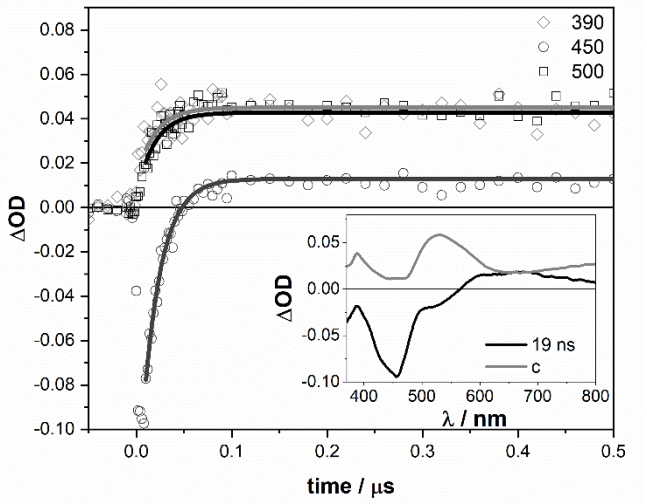

using a monoexponential function [$a_1\exp(-t/\tau)$ + c] and satisfactory fits gave a time constant of τ = 19 (± 3) ns corresponding to an apparent rate constant k_{app1} = 5.3 (± 0.3) × 10^7 s^{-1}. The decay-associated difference spectrum (DADS) with time constant 19 ns is attributed to the decay of Ru^{II}*-cT-Re^{I} together with the rise of Ru^{II}-cT-Re^{0} (shoulder at 520 nm) while the non-decaying component *c* is attributed to the spectrum of the 1st charge-separated state: $Asc^{\cdot+}$ and Ru^{II}-cT-Re^{0}. These species then undergo charge recombination at longer time scale occurring with a second order kinetic rate constant k_{rec2} = 9.6 (±1.0) × 10^8 $M^{-1}s^{-1}$ (Figure S2). The final ΔA_{509} = 0.07 corresponds to the formation of ~ 12.3 (±0.9) µM of Ru^{II}-cT-Re^{0} (using $\Delta\varepsilon$ = 5700 $m^{-1}cm^{-1}$),[41] that is 21 % of the ground state population.

Tracking the Second Charge Separated State (2nd CSS)

To investigate the second-electron accumulation in the Re moiety of the **Ru-cT-Re** dyad, a second nanosecond laser excitation was applied at 460 nm separated from the first excitation by 10 µs, a delay where the 1st CSS is optimal and the Ru photosensitizer is regenerated. The transient absorption spectra after the second laser excitation (Figure 5) did not show any new spectral changes compared to the changes after the first flash excitation (Figure 3). The transient absorption kinetics at short (Figure S3) and long time scale (Figure 6) show no significant differences compared to the first excitation indicating that a very similar charge transfer mechanism occurs upon second excitation. Of note, the doubly-reduced form of Re is expected to absorb at 570 nm with ε = 12100 $M^{-1}cm^{-1}$.[41] From the maximum ΔA_{509} = 0.06 after second excitation (Figure 5), the concentration of Ru^{II}-cT-Re^{0} created by the second pump is estimated to be 10.5 (± 0.9) µM, corresponding to 24% of the remaining ground state population, a very similar efficiency for the 1st CSS. In addition, the second order recombination rate is calculated to be k_{rec2} = 7.7 (±1.0) × 10^8 $M^{-1}s^{-1}$ (Figure 6 inset), closely similar to the one calculated for the first excitation.

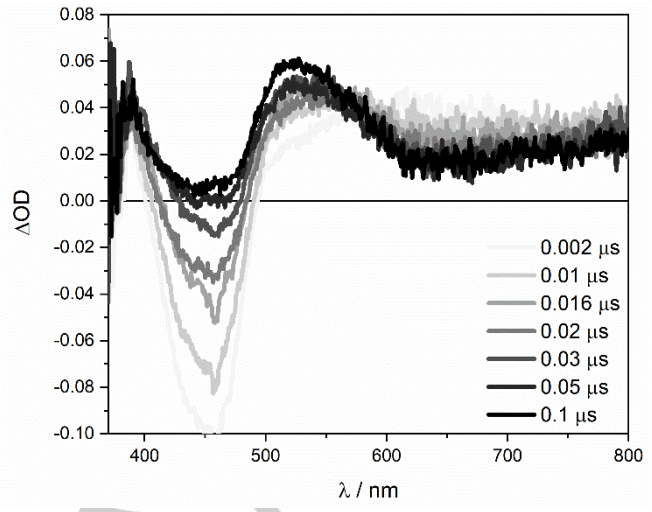

Figure 5. Transient absorption spectra of **Ru-cT-Re** (57 µM) and Asc (100 mM) in Ar-saturated ACN/H_2O in various delay times after double-pulse excitation at 460 nm delayed by 10 µs: first pump at 20 Hz, second pump at 10 Hz.

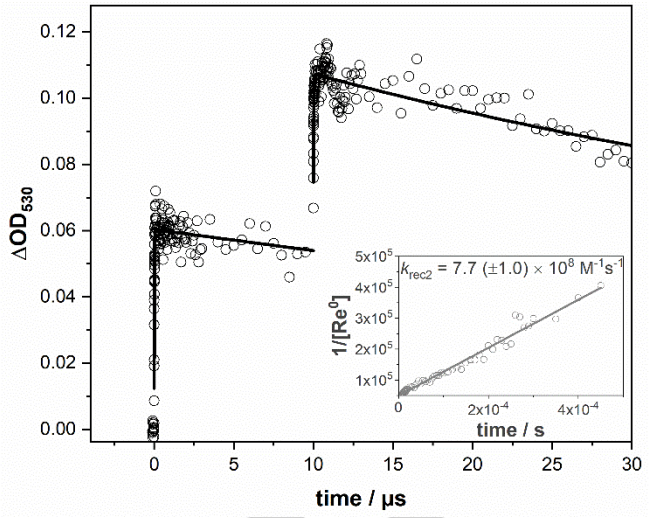

Figure 6. Transient absorption kinetics at 530 nm of **Ru-cT-Re** (57 µM) and Asc (100 mM) in Ar-saturated ACN/H_2O after first and second laser excitation at 460 nm. The effect of the first pump from 10 µs was added to the double pulse measurement to get the total quantity of the charge-separated state after the second pump. Inset: kinetic trace plotted as 1/[Re^0] *vs* time after double flash excitation.

Figure 7. Energy level diagram showing rate constants for the sequential charge accumulation in **Ru-cT-Re** dyad. Orange arrows: excitation; blue arrows: deactivation pathways; dashed arrows: recombination reaction; red arrows: unproductive competitive reactions; dotted level: expected states for 2nd CSS. The scheme is simplified for clarity: (i) changes in formal oxidation states are shown, (ii) involvement of Asc in (1, 4) and oxidized Asc^{+} in (6, 7, k_{rec1}, k_{rec2}) are not explicitly shown. Rate constants: k_{app1} ~ 5.4 (± 0.3) × 10^7 s^{-1} for steps (1) and (2) and k_{rec2} = 7.7 (± 1.0) × 10^8 $M^{-1}s^{-1}$.

These results indicate that excitation of the 1st CSS did not allow the formation of the accumulative charge transfer state under our conditions. This could be explained by a rapid quenching of Ru^{II}*-cT-Re^{0} by reverse electron transfer to form Ru^{I}-cT-Re^{I} (process 3 in Figure 7) followed by an intramolecular regeneration of the Ru^{II}-cT-Re^{0} state (process 2). All these intramolecular reactions are expected to be faster than the intermolecular quenching of Ru^{II}*-cT-Re^{0} by Asc to ideally create the two-electron accumulated form Ru^{II}-cT-Re^{-I} (k_3 >> k_{et2}). This

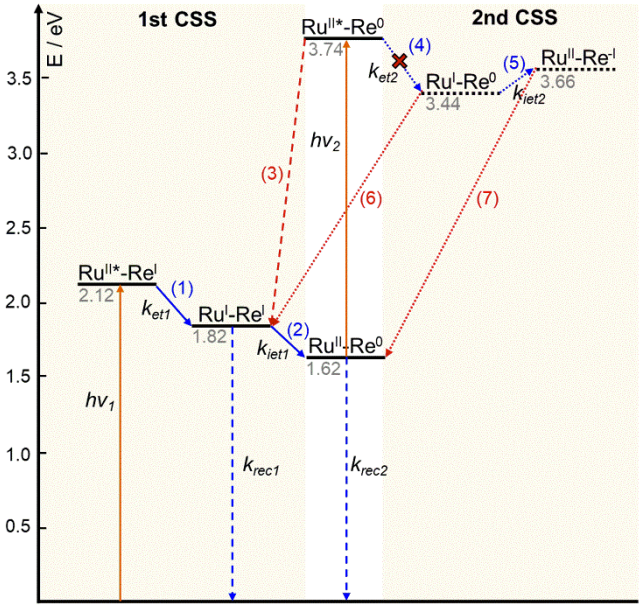

efficient reverse electron transfer have been similarly observed for other supramolecular systems in literature preventing the productive charge accumulation in catalytic/acceptor units.[42–47]

To avoid such intramolecular competitive unproductive pathway, a bimolecular system was also investigated and similar lack of charge accumulation on the **Re** catalyst was observed (Figure S4). This could come from the uphill thermodynamic drive (ΔG ~ +330 meV) for the electron transfer between Ru^{I} and Re^{0} to form Ru^{II} and Re^{-I}. A similar uphill thermodynamic drive (ΔG ~ +200 meV) is expected in the dyad to form Ru^{II}-cT-Re^{-I} (process 5) hinting to the eventual difficulty of photo-induced charge accumulation in the supramolecular system. Similar constraint can be expected for the other Ru-Re systems listed in Scheme 1 especially those that do not establish good electronic communication, as the relevant redox potentials would not be far from the bimolecular systems where the second electron accumulation in the Re from the Ru^{I} photo-reductant is highly endergonic.

Photocatalytic Activities

Even though photophysical investigation of the photo-induced processes in the **Ru-cT-Re** dyad subtly suggests the difficulty of two-electron accumulation in the **Re** moiety, under continuous illumination and use of sacrificial electron donors the system still shows the possibility of photocatalytic CO_2 reduction. The optimization of the photocatalytic conditions are presented in Table 3. From these optimizations, the following can be deduced: (i) the use of 1,3-dimethyl-2-phenylbenzimidazoline (BIH) as SED compared to 1-benzyl-1,4-dihydronicotinamide (BNAH) gave better photocatalytic activities mainly attributed to the high quenching efficiency of BIH (k_q = 3 × 10^9 $M^{-1}s^{-1}$) than BNAH (k_q = 3 × 10^8 $M^{-1}s^{-1}$)[40] and the participation of the highly reducing deprotonated oxidized radical [$E(BI^{\bullet})$ = -2.02 V *vs* $E(BNA^{\bullet})$ = -1.42 V vs Fc][11,13,48,49]; (ii) the TONs of the **Ru-cT-Re** dyad is inferior to its bimolecular counterpart, as similarly observed for other Ru-Re dyads allowing weak electronic communication[14,16]; and (iii) the introduction of the Ru photosensitizer, whether in bimolecular or supramolecular fashion, is always beneficial compared to using the Re catalyst alone as it provides sensitization in the visible region and the needed spatial and temporal separation of roles between photon capture, charge accumulation and catalysis.

The disparity between the investigation of the fast photo-induced processes and the photocatalytic performances of the **Ru-cT-Re** dyad and its bimolecular counterpart, highly suggests that despite efforts in establishing good thermodynamic photo-induced electron transfer from the photosensitizer to the catalyst for eventual charge accumulation and catalysis, the non-innocent role of the sacrificial electron donor plays critical role in determining the photocatalytic activities. We propose that for the **Ru-cT-Re** dyad and similar systems, the supramolecular assembly is beneficial in promoting a fast first photo-induced intramolecular electron transfer to accumulate the one-electron reduced species of the catalyst, but the eventual charge accumulation to form the more active doubly-reduced form of the catalyst is provided by a dark reaction from the radical by-product of the SED (Figure 8). The investigation is still open as to how supramolecular assemblies or sacrificial electron sources play further roles in the catalysis and how degradation mechanism alters photocatalytic performances. However, with the perspective that these supramolecular systems would be incorporated in a complete photo-electro-chemical cell with a thermodynamically favorable conveyance of electrons from the oxidation of water (void of any non-innocent highly reducing radicals), the design and thermodynamic requirements should be reconsidered to access the more catalytically active forms of the catalyst.

Table 3. Optimization of the reaction conditions for the photocatalytic CO_2 to CO reduction.

Entry	System[a]	SED[b]	Solvent[c]	µmol CO	TON[d]
1	**Ru-cT-Re**	Asc	DMF + 10% H_2O	-	-
2	**Ru-cT-Re**	BNAH	DMF	-	-
3	**Ru-cT-Re**	BNAH	DMF + TEOA	-	-
4	**Ru-cT-Re**	BNAH	DMF + 10% H_2O	0.6	5
5	**Ru + Re**	BNAH	DMF + 10% H_2O	1.2	8
6	**Re**	BNAH	DMF + 10% H_2O	0.3	3
7	**Ru-cT-Re**	BIH	DMF + 10% H_2O	38	257
8	**Ru + Re**	BIH	DMF + 10% H_2O	78	520
9	**Ru**	BIH	DMF + 10% H_2O	0.5	3
10	**Re**	BIH	DMF + 10% H_2O	5.6	37
11	**-**	BIH	DMF + 10% H_2O	-	-

[a] 50 µM concentration (equimolar when using bimolecular mixture), light source: LED lamp with λ_{em} = 463 nm (FWHM 50 nm, 180 W/m^2), 2 h irradiation. [b] SED = sacrificial electron donor, Asc = sodium ascorbate, BNAH = 1-benzyl-1,4-dihydronicotinamide, BIH = 1,3-dimethyl-2-phenylbenzimidazoline. [c] DMF=dimethylformamide, TEOA = triethanolamine, [d] TON calculated as moles of CO divided by moles of catalyst.

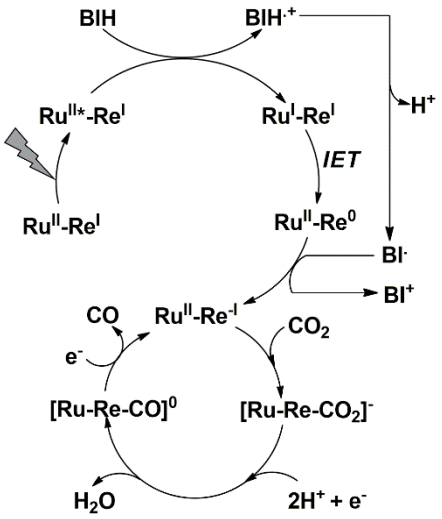

Figure 8. Proposed photocatalytic cycle for the **Ru-cT-Re** and similar systems. The e^- sources at the bottom cycle could come from either the Ru^{I} photoreductant or the highly reducing $BI^{\bullet}$.

Conclusion

The design of supramolecular assemblies bridging a photosensitizer unit and a catalytic unit is revisited in this study by investigating photo-induced electron transfer processes in a novel triazole-linked Ru-Re dyad. The triazole bridging ligand provided a weak electronic communication between the Ru and Re units with observed anodic shifts of the reduction potential of the latter. This resulted in a good thermodynamic drive (ΔG = -220 meV) for the 1st CSS forming a formal Ru^{II}-cT-Re^{0} occurring at a very fast apparent rate of k_{app1} = 5.4 (± 0.3) × 10^{7} s^{-1} as determined by nanosecond flash photolysis. The possibility of photo-induced two-electron accumulation in the Re moiety was tracked by a pump-pump-probe transient absorption technique but results show a competitive intramolecular reverse electron transfer just regenerating back the 1st CSS. The process of forming the more active doubly-reduced form of the Re catalyst is prevented by the highly endergonic process of electron transfer from the Ru^{I} photo-reductant, but can easily be overcome by using the non-innocent role of sacrificial electron donors providing highly reducing radical byproducts. The complementary and extensive investigations in this study point to substantial reconsiderations of supramolecular assembly design especially if such strategy will be employed in complete photo-electro-chemical cell applications.

Experimental Section

Synthesis of the reference compounds **Ru-cT-Ph**,[35] and **Re**,[50] as well as the necessary precursors (compounds **A** and **B**)[35] for "click" chemistry and sacrificial electron donors[48,51,52] are reported elsewhere. **Ru** photosensitizer was purchased from Sigma Aldrich in its dichloride form. All other chemical reagents used in the synthetic route were obtained from commercial sources as guaranteed-grade reagents and used without further purification. Water was Milli-Q filtered (18.2 MΩ· cm at 25 ° C). Proton and carbon nuclear magnetic resonance (^{1}H and ^{13}C NMR) spectra were recorded at room temperature on Bruker Advance spectrometers. The electrospray ionization mass spectrometry (ESI-HRMS) experiments were performed on TSQ (Thermo Scientific. 2009) with an ESI^{+} method. Ground state absorption spectra were measured on a Specord double beam spectrophotometer (Analytik Jena).

Synthesis of (bipyridine)$_2$-(bipyridine-triazol-bipyridine-N-oxide) ruthenium hexafluorophosphate (Compound C)

Compound **A** (203.2 mg, 0.23 mmol, 1.0 eq.) was suspended in CH_2Cl_2 (11.5 mL) under an argon atmosphere. Compound **B** (74.6 mg, 0.35 mmol, 1.5 eq.) was added, followed by successive addition of water (11.5 mL), sodium ascorbate (20.5 mg, 0.10 mmol, 0.45 eq.) and copper sulfate pentahydrate (8.6 mg, 0.03 mmol, 0.15 eq.). After 20 hours of stirring at room temperature, a saturated aqueous solution of ammonium hexafluorophosphate was added and the reaction mixture was extracted with CH_2Cl_2. The organic layers were washed with a saturated aqueous solution of NaCl, and concentrated. The crude solid was dissolved in a minimum amount of CH_2Cl_2 then filtered through an alumina plug. The excess of azido derivative was removed by washing with CH_2Cl_2, and the desired ruthenium complex was recovered by washing with CH_3CN and a solution of ammonium hexafluorophosphate in CH_3OH. The solvents were evaporated. The residue was dissolved in a minimum amount of CH_2Cl_2, then added drop wise at a large volume of pentane. The formed precipitate was filtered, washed several times with H_2O and Et_2O and dried under vacuum. **Yield:** 195.1 mg, 0.18 mmol, 77%. ^{1}H NMR (400 MHz, CD_3CN): δ = 9.15 (s, 1H), 8.98 (d, 1H, *J* =1.5 Hz), 8.92 (d, 1H, *J*=8.0 Hz), 8.80 (br s, 1H), 8.73 (d, 1H, *J*=3.2 Hz), 8.68 (br d, 1H, *J*=8.0 Hz), 8.55-8.47 (m, 4H), 8.44 (d, 1H, *J*=7.1 Hz), 8.11 (ddd, 1H, *J*=8.0, 7.9, 1.4 Hz), 8.11-8.03 (m, 4H), 8.02 (dd, 1H, *J*=8.0, 7.3 Hz), 7.94 (dd, 1H, *J*=7.1, 3.2 Hz), 7.86 (dd, 1H, *J*=5.9, 1.5 Hz), 7.86 (m, 1H), 7.81 (d, 1H, *J*=5.9 Hz), 7.79-7.73 (m, 4H), 7.56 (dd, 1H, *J*=7.3, 4.3 Hz), 7.46-7.38 (m, 5H) ^{13}C NMR (100 MHz, CD_3CN): δ = 159.1-158.2, 153.6, 153.1-153.0, 150.1, 149.7, 145.7, 144.9, 140.3, 139.2, 138.8, 129.2, 129.0, 126.9, 126.5, 125.9, 125.6, 124.3, 123.6, 121.4, 119.3, 118.6 HRMS (ESI^{+}) *m/z* calcd for $C_{42}H_{31}F_6N_{11}OPRu$: 952.1404; found: 952.1370; *m/z* calcd for $C_{42}H_{31}N_{11}ORu$: 403.5878; found: 403.5870.

Synthesis of ((bipyridine)$_2$-(bipyridine-triazol-bipyridine) ruthenium hexafluorophosphate (Compound D)

To a solution of ruthenium complex (compound **C**) (109.7 mg, 0.1 mmol, 1.0 eq.) in dry CH_2Cl_2 (20 mL) was added phosphorous trichloride (26 µL, 41.2 mg, 0.3 mmol, 3.0 eq.) at 0°C under an argon atmosphere. The reaction mixture was heated at reflux for 3 hours, then poured into an ice–water mixture and the pH of the aqueous phase was adjusted to 11 with an aqueous NaOH solution. The aqueous layer was extensively extracted with CH_2Cl_2. The organic layers were combined and washed with brine, then concentrated. The residue was dissolved in a minimum amount of CH_2Cl_2, then added dropwise at a large volume of pentane. The formed precipitate was filtered, washed several times with H_2O and Et_2O and dried under vacuum. **Yield:** 85.3 mg, 0.079 mmol, 79% ^{1}H NMR (400 MHz, CD_3CN) δ = 9.28 (s, 1H), 9.02 (d, 1H, *J*=1.7 Hz), 8.94 (d, 1H, *J*=2.1 Hz), 8.90 (d, 1H, *J*=5.3 Hz), 8.74 (br d, 1H, *J*=4.6 Hz), 8.70 (br d, 1H, *J*=8.1 Hz), 8.56-8.48 (m, 5H), 8.12 (ddd, 1H, *J*=8.1, 7.7, 1.3 Hz), 8.11-8.03 (m, 4H), 7.97 (ddd, 1H, *J*=7.8, 7.6, 1.3 Hz), 7.97 (dd, 1H, *J*=5.3, 2.1 Hz), 7.91 (dd, 1H, *J*=6.0, 1.7 Hz), 7.86 (br d, 1H, *J*=5.5 Hz), 7.82 (d, 1H, *J*=6.0 Hz), 7.79-7.73 (m, 4H), 7.49 (ddd, 1H, *J*=7.6, 4.6, 0.8 Hz), 7.46-7.38 (m, 5H) ^{13}C NMR (100 MHz, CD_3CN) δ = 159.8, 159.1, 158.3, 158.2, 155.9, 153.6, 153.2-153.1, 152.8, 150.9, 145.7, 145.4, 140.4, 139.2, 138.9, 129.2, 129.0, 126.3, 125.9, 125.7, 124.4, 123.7, 122.5, 121.5, 115.4, 111.9 HRMS (ESI^{+}) *m/z* calcd for $C_{42}H_{31}F_6N_{11}PRu$: 936.1454; found: 936.1436; *m/z* calcd for $C_{42}H_{31}N_{11}Ru$: 395.5904; found: 395.5903.

Synthesis of Ru-cT-Re

To a solution of ruthenium complex (compound **D**) (43.2 mg, 0.04 mmol, 1.0 eq.) in CH_3CN (7 mL) and THF (14 mL) was added bromopentacarbonylrhenium (I) (16.2 mg, 0.04 mmol, 1.0 eq.) at room temperature under an argon atmosphere. The reaction mixture was heated at 60°C for 18 hours, then the reaction mixture was concentrated. The residue was suspended in a mixture of CH_3OH and H_2O with hexafluorophosphate salt. The suspension was kept in the fridge overnight. The formed precipitate was filtered, washed several times with H_2O and Et_2O and dried under vacuum. **Yield**: 49.2 mg, 0.035 mmol, 86% ^{1}H NMR (400 MHz, CD_3CN) δ = 9.57 (s, 1H), 9.22 (d, 1H, *J*=6.2 Hz), 9.10 (d, 1H, *J*=1.4 Hz), 9.08 (ddd, 1H, *J*=5.5, 1.4, 0.6 Hz), 8.95 (d, 1H, *J*=1.9 Hz), 8.79 (br d, 1H, *J*=8.1 Hz), 8.70 (br d, 1H, *J*=8.2 Hz), 8.55-8.49 (m, 4H), 8.24 (ddd, 1H, *J*=8.2, 7.6, 1.4 Hz), 8.12 (ddd, 1H, *J*=8.1, 7.9, 1.4 Hz), 8.10 (dd, 1H, *J*=6.2, 1.9 Hz), 8.11-8.04 (m, 4H), 7.90 (dd, 1H, *J*=6.0, 1.4 Hz), 7.87 (ddd, 1H, *J*=5.8, 1.4, 0.7 Hz), 7.85 (d, 1H, *J*=6.0 Hz), 7.79-7.73 (m, 4H), 7.69 (ddd, 1H, *J*=7.6, 5.5, 1.0 Hz), 7.47-7.39 (m, 5H) ^{13}C NMR (100 MHz, CD_3CN) δ = 159.5, 159.3, 158.3, 158.3, 156.5, 156.3, 154.8, 153.8, 153.2-153.0, 146.2, 141.4, 139.9, 139.3, 129.6, 129.2, 129.0, 126.1, 126.0, 125.7, 124.4, 124.3, 121.6, 118.2, 115.3 HRMS (ESI^{+}) *m/z* calcd for $C_{45}H_{31}BrF_6N_{11}O_3PReRu$: 1286.0026; found: 1286.0079; *m/z* calcd for $C_{45}H_{31}BrN_{11}O_3ReRu$: 570.5189; found: 570.5221.

Electrochemical Characterization

Cyclic voltammetry measurements were performed in an electrochemical cell composed of a glassy carbon (3 mm diameter) working electrode, $Ag/AgNO_3$ (10^{-2} M) reference electrode, and a platinum wire counter electrode. Acetonitrile was mainly used as solvent and solutions of samples were prepared at a concentration of 1 mM. Tertbutylammonium hexafluorophosphate (TBAP) was used as supporting electrolyte and its concentration was maintained at hundredfold excess compared to the sample. The solutions were all purged with inert argon gas. Ferrocene was used as a reference for standard comparison in all experiments. Scan rate was chosen at 100 mV/s and a CH Instruments potentiostat

workstation was utilized to control the applied voltages and to measure resulting current.

Nanosecond Transient Absorption Spectroscopy

Single and double pump nanosecond transient absorption measurements were performed on a home-built set-up at which has been described in detail previously.[34] One or two Nd:YAG pumped optical parametric oscillator (OPO) lasers are used for sample excitation at 460 nm with an energy of ~6.5 mJ per pulse. The first pump operates at 20 Hz, whereas the second one has a repetition rate at 10 Hz. After excitation, the sample is probed with a pulsed nanosecond white light continuum laser at a repetition rate of 20 Hz. The probe beam is split into two arms, one for probing the sample and the other for reference in order to compensate for the pulse-to-pulse energy fluctuation. The probing arm after passing through the sample is coupled to a round to linear optical fiber bundle before being analyzed with a spectrograph SPEX 270 M (Jobin–Yvon). The detection of the dispersed white light is performed with an intensified CCD (ICCD) detector PIMAX 4 (Princeton Instrument). For the pump–probe experiments, only one excitation laser with a repetition rate at 10 Hz is employed. For the pump–pump–probe experiments, the setup is operated in the online subtraction mode in which the transient absorption after the first excitation is inherently removed by running the first pump at 20 Hz having the same repetition rate as the probe.

Photocatalytic Set-up and Product Characterization

Photocatalytic experiments were made in a modified quartz cuvette with a total volume of 6.85 mL, thermostated at 20°C, and sealed with a rubber septum. About 3.0 mL solutions of photocatalysts, and sacrificial electron donor were dissolved in appropriate solvents and were purged with CO_2 for 15 minutes. A SugarCUBE high intensity LED fiber optic illuminator was utilized with a blue light output centered at 463 nm with a full width at half maximum (FWHM) characteristic of about 50 nm. The source was adjusted to produce the lowest light intensity of 180 W/m^2 and the actual incident light power reaching the exposed cross section of the cuvette was 82 mW, as measured by a power meter. Gas chromatography was utilized to detect CO from the photocatalytic reduction of CO_2. For gas analysis, 50 uL gas aliquots were withdrawn from the head space of the cuvette with a gas-tight syringe and injected into the Trace GC Ultra, Thermo Scientific equipped with a 30 m molecular sieve porous layer open tubular (PLOT) column having an internal diameter of 0.53 nm, helium carrier gas, and a thermal conductivity detector (TCD). Peak separation between O_2, N_2, CO, and CO2 were achieved by programming the oven temperature from an initial 40 °C for 6 minutes, ramped by 20 °C/min until a final temperature of 250 °C held for 2 minutes. A splitless injector line was utilized to maximize the injection volume and become sensitive to possible trace amounts. A calibration curve relating peak area and concentration of CO was established by injecting known amounts of pure CO, and this calibration curve was used to determine actual amounts of CO produced. Turnover number (TON) was then calculated by dividing the moles of CO produced by the moles of catalyst consumed.

Acknowledgements

This work was supported by the French National Research Agency (ANR-19-CE05-0020-02, LOCO) and by the French Infrastructure for Integrated Structural Biology (FRISBI) ANR-10-INSB-05-01.

Keywords: carbon dioxide • rhenium catalyst • supramolecular chemistry • electron transfer • photocatalysis

[1] J. Hawecker, J.-M. Lehn, R. Ziessel, *J. Chem. Soc., Chem. Commun.* **1983**, 536–538.
[2] J. Hawecker, J.-M. Lehn, R. Ziessel, *Helvetica chimica acta* **1986**, *69*, 1990–2012.
[3] J. M. Smieja, E. E. Benson, B. Kumar, K. A. Grice, C. S. Seu, A. J. M. Miller, J. M. Mayer, C. P. Kubiak, *Proc. Natl. Acad. Sci. USA* **2012**, *109*, 15646–15650.
[4] H. Hori, K. Koike, M. Ishizuka, K. Takeuchi, T. Ibusuki, O. Ishitani, *J. Organomet. Chem.* **1997**, *530*, 169–176.
[5] H. Tsubaki, S. Tohyama, K. Koike, H. Saitoh, O. Ishitani, *Dalton Trans.* **2005**, *0*, 385–395.
[6] H. Tsubaki, A. Sekine, Y. Ohashi, K. Koike, H. Takeda, O. Ishitani, *J. Am. Chem. Soc.* **2005**, *127*, 15544–15555.
[7] P. Kurz, B. Probst, B. Spingler, R. Alberto, *European Journal of Inorganic Chemistry* **2006**, *2006*, 2966–2974.
[8] H. Takeda, K. Koike, H. Inoue, O. Ishitani, *J. Am. Chem. Soc.* **2008**, *130*, 2023–2031.
[9] J. M. Smieja, C. P. Kubiak, *Inorg. Chem.* **2010**, *49*, 9283–9289.
[10] A. J. Huckaba, E. A. Sharpe, J. H. Delcamp, *Inorg. Chem.* **2016**, *55*, 682–690.
[11] Y. Yamazaki, H. Takeda, O. Ishitani, *J. Photochem. Photobiol. C* **2015**, *25*, 106–137.
[12] Y. Tamaki, O. Ishitani, *ACS Catal.* **2017**, *7*, 3394–3409.
[13] Y. Tamaki, K. Koike, T. Morimoto, O. Ishitani, *J. Catal.* **2013**, *304*, 22–28.
[14] Z.-Y. Bian, S.-M. Chi, L. Li, W. Fu, *Dalton Trans.* **2010**, *39*, 7884.
[15] Z.-Y. Bian, H. Wang, W.-F. Fu, L. Li, A.-Z. Ding, *Polyhedron* **2012**, *32*, 78–85.
[16] B. Gholamkhass, H. Mametsuka, K. Koike, T. Tanabe, M. Furue, O. Ishitani, *Inorg. Chem.* **2005**, *44*, 2326–2336.
[17] S. Meister, R. O. Reithmeier, A. Ogrodnik, B. Rieger, *ChemCatChem* **2015**, *7*, 3562–3569.
[18] S. Sato, K. Koike, H. Inoue, O. Ishitani, *Photochem. Photobiol. Sci.* **2007**, *6*, 454–461.
[19] Z.-Y. Bian, K. Sumi, M. Furue, S. Sato, K. Koike, O. Ishitani, *Dalton Trans.* **2009**, 983–993.
[20] K. Koike, S. Naito, S. Sato, Y. Tamaki, O. Ishitani, *J. Photochem. Photobiol. A* **2009**, *207*, 109–114.
[21] Y. Yamamoto, Y. Tamaki, T. Yui, K. Koike, O. Ishitani, *Journal of the American Chemical Society* **2010**, *132*, 11743–11752.
[22] A. Nakada, K. Koike, T. Nakashima, T. Morimoto, O. Ishitani, *Inorg. Chem.* **2015**, *54*, 1800–1807.
[23] Y. Ueda, H. Takeda, T. Yui, K. Koike, Y. Goto, S. Inagaki, O. Ishitani, *ChemSusChem* **2015**, *8*, 439–442.
[24] T. L. Easun, W. Z. Alsindi, M. Towrie, K. L. Ronayne, X.-Z. Sun, M. D. Ward, M. W. George, *Inorg. Chem.* **2008**, *47*, 5071–5078.
[25] K. Koike, D. C. Grills, Y. Tamaki, E. Fujita, K. Okubo, Y. Yamazaki, M. Saigo, T. Mukuta, K. Onda, O. Ishitani, *Chem. Sci.* **2018**, *9*, 2961–2974.
[26] L. Frayne, N. Das, A. Paul, S. Amirjalayer, W. J. Buma, S. Woutersen, C. Long, J. G. Vos, M. T. Pryce, *ChemPhotoChem* **2018**, *2*, 323–331.
[27] E. Kato, H. Takeda, K. Koike, K. Ohkubo, O. Ishitani, *Chem. Sci.* **2015**, *6*, 3003–3012.
[28] C. M. Brown, T. Auvray, E. E. DeLuca, M. B. Ezhova, G. S. Hanan, M. O. Wolf, *Chem. Commun.* **2020**, *56*, 10750–10753.
[29] F. P. A. Johnson, M. W. George, F. Hartl, J. J. Turner, *Organometallics* **1996**, *15*, 3374–3387.
[30] P. Christensen, A. Hamnett, A. V. G. Muir, J. A. Timney, *Journal of the Chemical Society, Dalton Transactions* **1992**, *0*, 1455–1463.
[31] B. P. Sullivan, C. M. Bolinger, D. Conrad, W. J. Vining, T. J. Meyer, *J. Chem. Soc., Chem. Commun.* **1985**, *0*, 1414–1416.
[32] H. C. Kolb, M. G. Finn, K. B. Sharpless, *Angewandte Chemie International Edition* **2001**, *40*, 2004–2021.
[33] A. Baron, C. Herrero, A. Quaranta, M.-F. Charlot, W. Leibl, B. Vauzeilles, A. Aukauloo, *Chem. Commun.* **2011**, *47*, 11011–11013.
[34] S. Mendes Marinho, M.-H. Ha-Thi, V.-T. Pham, A. Quaranta, T. Pino, C. Lefumeux, T. Chamaillé, W. Leibl, A. Aukauloo, *Angew. Chem. Int. Ed.* **2017**, *56*, 15936–15940.
[35] A. Baron, C. Herrero, A. Quaranta, M.-F. Charlot, W. Leibl, B. Vauzeilles, A. Aukauloo, *Inorg. Chem.* **2012**, *51*, 5985–5987.
[36] C. Herrero, A. Quaranta, M. Sircoglou, K. Sénéchal-David, A. Baron, I. M. Marín, C. Buron, J.-P. Baltaze, W. Leibl, A. Aukauloo, F. Banse, *Chem. Sci.* **2015**, *6*, 2323–2327.
[37] C. Herrero, A. Quaranta, S. El Ghachtouli, B. Vauzeilles, W. Leibl, A. Aukauloo, *Physical Chemistry Chemical Physics* **2014**, *16*, 12067.
[38] A. Juris, V. Balzani, F. Barigelletti, S. Campagna, P. l Belser, A. Von Zelewsky, *Coordination Chemistry Reviews* **1988**, *84*, 85–277.
[39] K. Kalyanasundaram, *J. Chem. Soc., Faraday Trans. 2* **1986**, *82*, 2401–2415.
[40] P. Gotico, A. Del Vecchio, D. Audisio, A. Quaranta, Z. Halime, W. Leibl, A. Aukauloo, *ChemPhotoChem* **2018**, *2*, 715–719.
[41] Y. F. Lee, J. R. Kirchhoff, R. M. Berger, D. Gosztola, *J. Chem. Soc., Dalton Trans.* **1995**, *0*, 3677–3682.
[42] L. Hammarström, *Acc. Chem. Res.* **2015**, *48*, 840–850.

[43] R. Lomoth, T. Häupl, O. Johansson, L. Hammarström, *Chemistry – A European Journal* **2002**, *8*, 102–110.
[44] L. Flamigni, E. Baranoff, J.-P. Collin, J.-P. Sauvage, B. Ventura, *ChemPhysChem* **2007**, *8*, 1943–1949.
[45] M. Kuss- Petermann, O. S. Wenger, *Helvetica Chimica Acta* **2017**, *100*, DOI 10.1002/hlca.201600283.
[46] M. Skaisgirski, X. Guo, O. S. Wenger, *Inorg. Chem.* **2017**, *56*, 2432–2439.
[47] M.-H. Ha-Thi, V.-T. Pham, T. Pino, V. Maslova, A. Quaranta, C. Lefumeux, W. Leibl, A. Aukauloo, *Photochem. Photobiol. Sci.* **2018**, *17*, 903–909.
[48] X.-Q. Zhu, M.-T. Zhang, A. Yu, C.-H. Wang, J.-P. Cheng, *J. Am. Chem. Soc.* **2008**, *130*, 2501–2516.
[49] Y. Pellegrin, F. Odobel, *Comptes Rendus Chimie* **2017**, *20*, 283–295.
[50] E. Portenkirchner, K. Oppelt, C. Ulbricht, D. A. M. Egbe, H. Neugebauer, G. Knör, N. S. Sariciftci, *Journal of Organometallic Chemistry* **2012**, *716*, 19–25.
[51] D. Mauzerall, F. H. Westheimer, *J. Am. Chem. Soc.* **1955**, *77*, 2261–2264.
[52] E. Hasegawa, T. Seida, N. Chiba, T. Takahashi, H. Ikeda, *J. Org. Chem.* **2005**, *70*, 9632–9635.

Entry for the Table of Contents

Insert graphic for Table of Contents here.

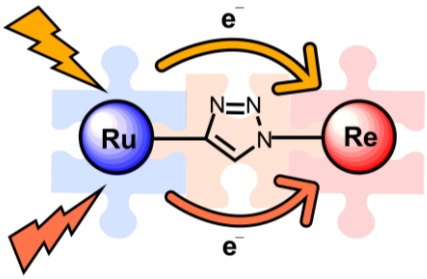

A dyad consisting of a ruthenium photosensitizer linked to a rhenium catalyst by a triazole bridge was scrutinized for photo-induced charge accumulation. A first charge-separated state was formed upon excitation and intramolecular electron transfer, but second excitation did not allow charge accumulation. Regardless, the dyad showed good photocatalytic activity towards CO_2 reduction, hinting the non-innocent role of byproducts in solution.

Institute and/or researcher Twitter usernames: **@CEA_Joliot, @I2BCParisSaclay, @ISMOlab_Orsay, @UnivParisSaclay**